ELSEVIER

Surface and Coatings Technology 139 (2001) 63–74

SURFACE & COATINGS TECHNOLOGY

www.elsevier.nl/locate/surfcoat

Indentation hardness evaluation of cathodic arc deposited thin hard coatings

J.R. Tuck[a,b], A.M. Korsunsky[b,*], D.G. Bhat[c,1], S.J. Bull[a]

[a] *Department of Mechanical, Materials and Manufacturing Engineering, University of Newcastle, Newcastle upon Tyne NE1 7RU, UK*
[b] *Department of Engineering Science, University of Oxford, Parks Road, Oxford OX1 3PJ, UK*
[c] *Stellram Inc., La Vergne, TN, USA*

Received 21 July 2000; accepted in revised form 12 October 2000

Abstract

One trend in the development of wear-resistant vapour deposited coatings is to make them increasingly harder and thinner, by improvement and optimisation of the deposition processes. A complex interdependence exists between the individual properties of a coating and a substrate on the one hand, and those of the 'composite' coated system on the other. For example, system stiffness and hardness may vary with indentation depth according to different laws. There is a great need for quantitative modelling methods so that the design of coatings and multi-layered systems can be improved, and the choice of materials optimised. In the present study, various hard coatings produced by filtered cathodic arc deposition were characterised by micro-indentation and macro-indentation methods, and scanning electron microscopy. SEM was used to elucidate the fracture behaviour of these coatings, which exerts an important influence on their hardness performance. Hardness testing results were analysed using a newly proposed modification of the work-of-indentation model, an approach that was recently developed and applied to a range of coated systems. The new development of this model allows more accurate fitting of the empirical data, and yields an estimate for the ultimate coating hardness, and values of dimensionless materials parameters β_0 and X. These parameters describe the normalised depth and the degree of abruptness at which the hardness transition from coating to substrate occurs, and are related in a complex way to the ductility and toughness of the thin film and the interface, as well as the substrate's yield strength and hardening behaviour. In this study we use the model to interpret micro- and macro-indentation data, and to discuss the results of extrapolating the depth–hardness curve to the important region where the indentation depth lies is between 5 and 10% of the coating thickness, and composite hardness approaches the ultimate film hardness.

Keywords: Characterisation models (X); Vickers hardness test (B); Scanning electron microscopy (B); Cathodic arc evaporation (C); Titanium nitride (D); Zirconium nitride (D)

1. Introduction

Coated systems, particularly those used on hard metals for cutting tools, have produced a remarkable enhancement in productivity since their wide introduction in the late 1960s and early 1970s. Since then, these coatings have been developed as a surface engineering enhancement solution for cutting tools, dies, drills and other tribological applications, all of which utilise the fact that the coating materials are extremely hard and abrasion resistant. In cutting tools applications, the coatings also act as diffusion barriers that isolate the chip formed on the work piece from the cutting material itself, and allow much higher cutting speeds than would be possible of the bulk material alone [1].

Increasingly, thin, hard coatings such as PVD deposited nitrides considered in this study, are becoming widespread in industrial applications [2]. As the coatings become harder and, in some instances, thinner,

* Corresponding author. Tel.: +44-1865-273043; fax: +44-1865-273010.
E-mail address: alexander.korsunsky@eng.ox.ac.uk (A.M. Korsunsky).
[1] Formerly UES Arcomac Inc., Dayton, OH, USA.

0257-8972/01/$ - see front matter
PII: S0257-8972(00)01116-6

and the deposition processes are optimised, the application requirements become more stringent and specific. There arise the linked requirements to characterise these advanced systems, and to understand more fully their response to contact loading and wear. It is desirable that this characterisation procedure is relatively simple, non-destructive, and cost-effective. Furthermore, for the purposes of industrial implementation it must be possible to perform such tests on the shop floor or in an industrial laboratory.

Composite hardness modelling has been studied since the 1970s; Jonsson and Hogmark [3] proposed a simple composite hardness relation based on area functions of the film and substrate. Two variations were proposed, either with the film bending under strain to match the indenter shape, or cracking within the indentation zone. They concluded that the former model (where the film bends to match the indenter shape) would be more applicable to deformation involving harder substrates whilst the latter would be a better description of the deformation of coatings on softer substrates. It was also established that the modelling works well for indentations of depth not less than the coating thickness.

The volume law-of-mixtures model, originally suggested by Sargent [4], was taken further by Burnett and Rickerby [5], and Burnett and Page [6]. They used Marsh's expanding spherical cavity model [7] coupled with the intuitive observation that a hard coating with a higher yield stress, which is well bonded to the substrate, will not yield before the softer substrate, and in consequence will be pushed down into it. The deformation pattern beneath the indenter is based on a hemispherical shape, and by calculating the volumes of the portions of the total deforming volume that lies in the coating and substrate, V_f and V_s, respectively, the composite hardness, H_c could be expressed for the case $H_f > H_s$, as

$$H_c = \frac{V_f}{V} H_f + \frac{V_s}{V} \chi^3 H_s \tag{1}$$

where the total deforming volume is $V = V_f + \Phi^3 V_s$. Here, H_f and H_s are the hardness of the film and substrate, respectively, and Φ is a function of the coating and substrate elastic and plastic properties,

$$\chi \alpha \left(\frac{E_f}{E_s} \Big/ \frac{H_f}{H_s} \right)^{\frac{n}{2}} \tag{2}$$

where χ and n are empirically derived parameters. Different plastic zone configurations are likely to be realised depending on whether the parameter χ is less or greater than unity. The two prominent cases are shown in Fig. 1.

Bull and Rickerby [8] described procedures for the accurate determination of χ and n and incorporate a more realistic appraisal of the coating behaviour directly below the indenter. They concluded that the break up of the coating (as noted by Jonsson and Hogmark) within the indentation rendered quite impractical any attempt to reliably obtain an accurate measure of the deforming volumes involved. The approach remained satisfactory for thick coatings.

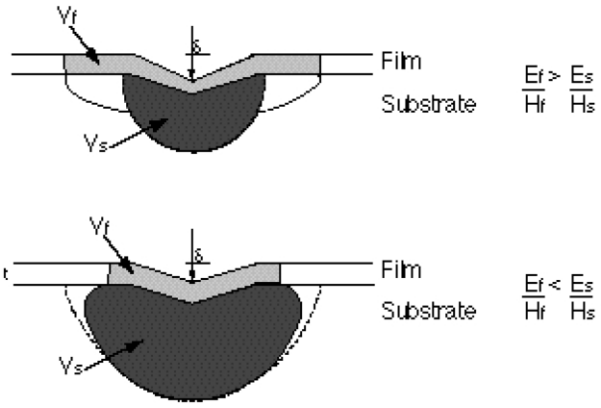

Fig. 1. Relative plastic zones volumes envisaged for the volume law-of-mixtures proposed by Burnett and Rickerby [5].

The development of surface engineering over the following decades followed the path toward thinner coatings, which possessed finer and more uniform microstructure, and as a consequence displayed higher yield stress and hardness. Plastic deformation always takes place in the nearest vicinity of the indenter tip even in these systems, where the deformation is highly constrained by the surrounding material, and a state of high hydrostatic compression results. However, high hardness is usually associated with limited ductility, and the thin coating layer around the periphery of the contact zone undergoes strong bending, and fracture. This mode of response dominates the behaviour of hard-coated systems under most conditions, extremely sharp indenters and very low loads being excepted. It is therefore essential to develop a modelling methodology that allows this deformation mechanism to be incorporated in the analysis.

Recently, a number of attempts have been made [9–11] to develop a sufficiently general analysis of coated system indentation, based on the concept of work-of-indentation. The general idea, of course, is not new, and goes back to the views of Tabor [12]. However, the remarkable utility of this approach in application to the coated systems is that it allows any mechanism of energy expenditure, be it though-thickness coating cracking, substrate-coating interface delamination, or plastic flow, to be incorporated in the same analysis. Of course, if the specific parameters characterising each of these phenomena are required to be determined, then the problem of de-coupling their influences arises. Nevertheless, even using generic argu-

ments based on dimensional analysis and work partitioning between the substrate and the coating, it is possible to identify the general form of the function that describes the apparent hardness variation with increasing load or indentation depth.

The application of the work-of-indentation modelling to PVD nitrides on steel substrates, as well as DLC coatings, electroplated nickel coatings on copper substrates, etc. [9–11,13,14] has shown that it is possible to predict the indentation response of coated systems during indentation ranging from macro (100–10 N), through micro indentation (10–150 mN), to nano indentation (500–1 mN). The modelling approach has been shown to be effective for both soft-on-hard and hard-on-soft systems, and capable of dealing with the mixed deformation responses (plastic flow, cracking and interfacial delamination).

The fundamental result obtained from the work-of-indentation approach was that the response can be predicted accurately using modelling in the form [9]:

$$H_c = H_s + \frac{H_f - H_s}{1 + k\beta^2} \tag{3}$$

where H_c is the apparent composite hardness, H_f is the intrinsic film hardness, H_s is the substrate hardness, k is a dimensionless materials parameter related to the composite response mode to indentation. The key variable in the above formula is β, the relative indentation depth (RID), defined as the ratio of the maximum indenter penetration depth to the coating thickness.

It is clear from the above formulation that the precise nature of the parameter β depends on the definition of indentation depth itself, and hence on the nature of the indentation experiment. For example, in a nanoindentation experiment the total indenter displacement is recorded, while the 'contact area' and 'contact depth' are parameters that cannot be determined directly from the experiment. However, they are required in order to evaluate hardness, and for this purpose usually found based on the assumption of elastic composite behaviour during the initial stage of unloading.

In conventional Vickers macro and microhardness indentation testing, the maximum contact depth can be estimated from the knowledge of the indentation diagonal and indenter tip shape (depth = diagonal/7). An important assumption implicit in this argument is that the visible diagonal represents the full extent of contact under maximum load, i.e. that permanent plastic deformation of the coating took place throughout the contact, and that the amount of elastic recovery of the diagonal length during unloading is negligible. In the interpretation of microhardness experiments carried out within the present study we used this method of defining the indentation depth.

Work-of-indentation modelling has previously shown that the undesirable effects on hardness interpretation of pile-up and sink-in can be minimised using this approach [14].

A further development of the work-of-indentation formula (3) is introduced in the present study. It was found that in its present form the formula is incapable of capturing the full extent of hardness response variation. The restriction arises due to the fact that the parameter β enters the formula in the form of its square, β^2. However, an analysis of cracking during indentation under intermediate to large loads [11] suggests that it may have to be replaced with a term of power 1 to achieve better agreement. Furthermore, a full range of values of the power exponent must be accessible to describe the transition.

In this paper therefore we aim to present a different approach to the work-of-indentation based modelling that provides better agreement between the fit and the empirical data. The hardness data was obtained from a set of standard coated samples produced by filtered cathodic arc at UES Arcomac, Inc. We discuss the interpretation of the newly introduced parameters E_0 and X, and show that a better prediction of the ultimate film hardness in a thin film coated system is obtained.

Filtered cathodic arc deposition has a wide range of applications including conventional cutting tools, dies and drills. The process is characterised by the high deposition rate, and allows large areas to be coated. Filtering eliminates an important shortcoming of the process, namely the fact that a large fraction of the mass is deposited in the form of macro-particles, when the metal plasma flux is not filtered effectively. The process can produce coatings with very low coefficient of friction, for example TiN + diamond-like carbon (DLC), thermal barrier coatings such as Al_2O_3 + NiCrAlY, used on aeroengine turbine blades, Si for Silicon wafers in the electronics industry and DLC for hard drive manufacture.

2. Deposition process and testing procedure

Polished discs (19 mm in diameter × 5 mm thick) of heat-treated M2 tool steel were used as substrate material. A blind hole, of length approximately equal to the radius of the disc, and of diameter approximately half of the disk thickness, was spark eroded into the side of the disc for mounting in the chamber. The substrates were cleaned ultrasonically in acetone and isopropyl alcohol before placing into the deposition chamber. All coatings were deposited in the LAFAD™ system at

UES Inc. The substrates were mounted on a variable speed substrate holder with double planetary rotation capability that can be biased to a desired voltage using either a bipolar DC pulse or RF power supply.

Arc plasma was generated by a patented electronic trigger and controlled by an arc spot circuitry that effectively eliminates the tendency of arc spot to be extinguished and provides continuous stable operation over extended periods.

The deposition chamber was evacuated to a pressure of 7×10^{-4} Pa prior to the introduction of gases such as argon, nitrogen and methane. The coating process consisted of substrate sputter cleaning, deposition of metal bond layer, and deposition of the coating. Substrate cleaning was done in Ar plasma aided by the electrons from the arc sources. Plasma cleaning was done for a time period of 3 min at substrate temperature of approximately 370°C. After the initial metal bond layer was applied, TiN, CrN, ZrN coatings were deposited employing Ti, Cr and Zr cathodes, respectively, in filtered arc mode in nitrogen atmosphere.

TiCN coating was deposited using Ti cathodes in a mixed atmosphere of nitrogen and methane. Carbon and nitrogen content in the TiCN coating was varied by adjusting the flow rates of nitrogen and methane gases. Multilayer Ti/TiCN coatings were deposited by switching the atmosphere from argon to methane/nitrogen mixture. Typical working pressure, substrate bias, substrate temperature for these coatings were in the range of 10^{-2} to 10^{-1} Pa, -40 to -100 V and 350–400°C, respectively.

Thickness of the coatings produced varied between 1 and 4 μm, approximately. Precise values were determined by ball cratering. Table 1 lists the materials and thickness of the coatings used in the present study.

The hardness of all systems was tested using Vickers microhardness testers (Shimadzu and Buehler Micromet) and standard macro indentation machines. Three indents were used for each load, recovering six indent diagonals from which an average was taken. Care was taken to ensure that at least five indent sizes were left between each indent in order for one not to influence the response of another. Note that the results obtained through macro-indentation were clearly affected by use of a blunt indenter, which significantly raised the estimated substrate hardness in each case. Subsequently a sharp indenter was used for all measurements.

For the purposes of comparison, ultra-low load hardness testing was also performed using Nanoindenter II™.

The indents were imaged using secondary and backscattered electrons in the SEM, in order to observe the indentation response of the coated system, confirming that significant fracture occurred during the higher loading of the micro scale range.

3. Work of indentation analysis

One of the striking characteristics of coated systems is the dependence of their hardness on the applied load, or indenter depth. This dependence means that simply quoting the value of system hardness at any given load is not sufficient to describe the response fully. In order to appreciate this, it is convenient to introduce a dimensionless length scale parameter, called the relative indentation depth (RID), denoted β.

When hardness is plotted against RID, as shown in Fig. 2 for a 2.8-μm NbN coating on M304 stainless steel, the graph may appear similar to the indentation size effect, where H grows without obvious limit. However, when a logarithmic scale is used for RID, a characteristic knee shaped profile is observed as shown in Fig. 3, plotted using the same data as above. This profile allows us to assess the full range of system hardness, as depending upon the thickness of the coating; a hardness test at any one load could put us

Table 1
Hardness of PVD nitride coatings on M2 tool steel substrates, characterised over the entire micro/macro range of relative indentation depth[a]

Sample	t (μm)	$Hv_{0.1}$ (GPa)	H_f, (GPa)	H_s, GPa	k	X	X error	β_0	β_0 error	$\beta_{2/3}$
$TiN_{(1A)}$	3.5	17.8	32.3	9.0	7.78	1.92	0.19	0.34	0.02	0.09
$TiN_{(1A)}$	**3.5**	**17.8**	**32.4**	**9.2**	**11.43**	**1.67**	**0.30**	**0.23**	**0.03**	**0.07**
$TiN_{(1B)}$	3.25	16.1	23.1	8.8	4.12	1.92	0.11	0.48	0.02	0.13
$TiN_{(3)}$	**3.75**	**14.5**	**27.7**	**7.6**	**8.41**	**1.73**	**0.12**	**0.29**	**0.01**	**0.09**
$TiN_{(1C)}$	3.6	15.2	29.9	8.9	10.9	1.96	0.22	0.30	0.02	0.08
$TiN_{(1C)}$	**3.6**	**15.2**	**32.3**	**8.8**	**12.6**	**1.45**	**0.23**	**0.18**	**0.03**	**0.06**
$TiCN_{(2C)}$	3.25	18.1	56.1	8.2	15.84	1.87	0.28	0.23	0.02	0.06
$ZrN_{(1)}$	**4.4**	**14.9**	**23.7**	**9.3**	**10.91**	**2.12**	**0.45**	**0.32**	**0.04**	**0.07**
$ZrN_{(2)}$	**4**	**13.6**	**15.7**	**8.7**	**3.27**	**2.44**	**0.37**	**0.62**	**0.04**	**0.11**
$ZrN_{(3)}$	**3.75**	**15.7**	**28.4**	**8.9**	**7.82**	**1.74**	**0.16**	**0.31**	**0.02**	**0.09**

[a] Two different micro hardness testers were used. The results produced using the Buehler tester are shown in bold. The rest of the results were obtained using a Shimadzu tester. Standard Vickers macro-hardness testers were used for higher load indentation.

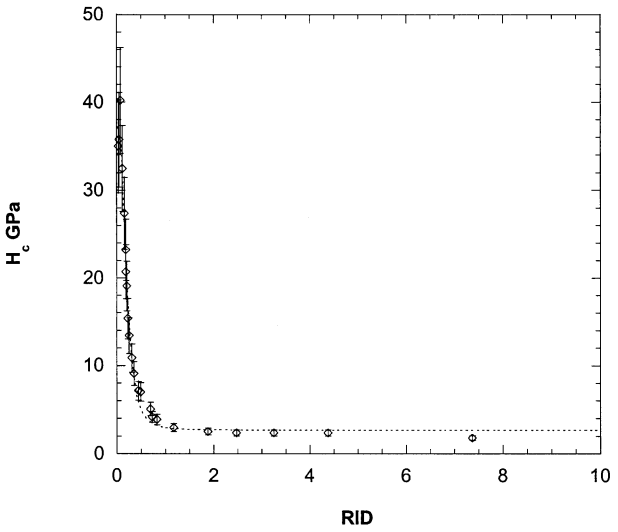

Fig. 2. Composite hardness plotted against RID for a 2.8-μm NbN coating on M304 steel. The curve fit resolves values of $H_s = 2.7$ GPa, $H_f = 37.8$ GPa, $k = 115.3$ and $X = 3$.

anywhere along this curve. It is therefore necessary to investigate what happens over the whole range of RID.

It is interesting to study the modes of response as they evolve, with increasing RID, in more detail. Fig. 4 is a diagram presented by Korsunsky et al. [9], showing a schematic representation of such evolution. It is seen that coating plasticity dominates the response at low loads, but with increasing penetration, coating fracture

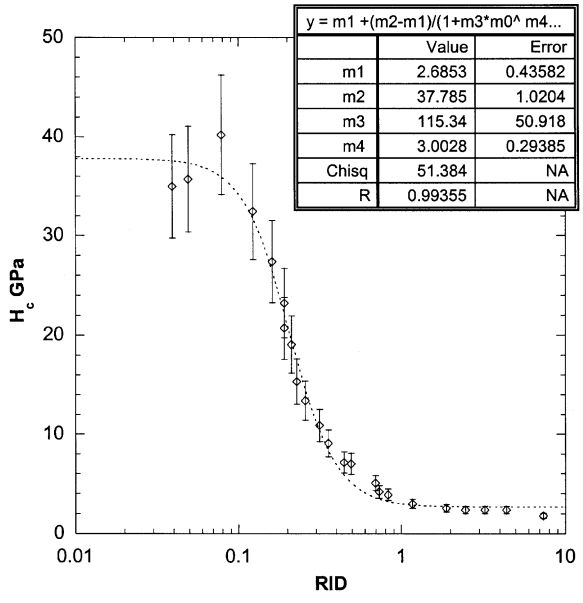

Fig. 3. Composite hardness for a 2.8-μm NbN coating on M304 steel plotted against the log of relative indentation depth (RID). It can clearly be seen from this plot that, depending on the coating thickness, a hardness test at any one load could yield a result anywhere along that curve, and in the hardness range between the maximum and minimum bounds.

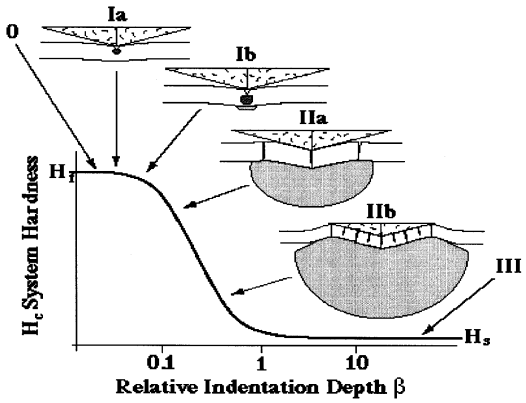

Fig. 4. A schematic showing the evolution of fracture and plastic response of a coated system, as the load is increased during indentation.

becomes the main response mode. This process can be separated into three main stages. At stage I, local plasticity in the film and substrate are observed. At stage II, coating cracking sets in, and a system of concentric cracks develops. Finally, at stage III, coating fragmentation is extensive, and hardness falls to values close to that of the substrate.

Under the lowest loads (stage I), and in the absence of fracture under the indenter, hard surface films display localised plastic flow within the region of highly compressive three-dimensional state of stress immediately under the indenter. As loading progresses, the film undergoes membrane flexure, which acts to redistribute the pressure away from the contact patch, thus reducing the propensity of the substrate to flow. The situation is changed abruptly once a critical load is reached, and the first circumferential through-thickness crack develops. This phenomenon is responsible for the frequently observed displacement discontinuity on the load–displacement curve. Methods of film toughness evaluation have been proposed [15] which are based on the value of the critical load. However, the latter may be strongly dependent on the indenter shape, as well as the presence and location of individual flaws within the film, etc.

In the present study we explore an alternative approach which allows to include in the consideration the case of fracture dominated response of the coating, as seen in stages II and III (Fig. 4). As the indenter load is increased beyond the critical value, discontinuities in the load–displacement trace disappear, but hardness continues to drop until the uncoated substrate hardness is almost completely recovered for RID $\gg 1$. The total energy expenditure during indentation can be partitioned into the contributions made by substrate plasticity and coating cracking. A formula more general than (3) can be constructed in order to describe the variation of system hardness H with the RID β, in the form similar to (3) where an arbitrary power exponent

X of the parameter E is introduced:

$$H = H_s + \frac{H_f - H_s}{1 + k\beta^X} \tag{4}$$

Here H_s and H_f are the intrinsic substrate and film hardness respectively, k is a dimensionless hardness transition parameter, and X is the power exponent that depends on the deformation mode and geometry. As an example of this, the curve in Fig. 3 represents the best fit of Eq. (4) to the data from indentation of a 2.8-μm NbN coating on M304 steel as a plot of composite hardness against RID, β.

Once the variation of the power exponent is allowed in the fit, the values of the parameter k become very dependent on the choice of X. Also, comparison of parameter k between fits which led to different values of X becomes meaningless. Thus, for the purposes of analysis, comparison and discussion, it is convenient to introduce, instead of k, another parameter, denoted β_0:

$$H = H_s + \frac{H_f - H_s}{1 + (\beta/\beta_0)^X} \tag{5}$$

where $k = \beta_0^{-X}$.

For the purposes of this discussion Eq. (5) can be re-written in the form

$$\frac{H - H_s}{H_f - H_s} = \frac{1}{1 + (\beta/\beta_0)^X} \tag{6}$$

Now the expression in the left hand side represents the apparent hardness improvement, as a fraction of the maximum achievable with the given coating and substrate intrinsic hardnesses. This fraction increases from zero under very large load to the maximum of unity under ultra-low loads.

The expression in the right hand side is a function of the relative indentation depth β, and contains β_0 and X as parameters. Eq. (6) thus provides a means of expressing the fractional hardness improvement as a function of indentation depth over the entire range of loads. Note that the coating thickness does not appear in the formula on its own, but only in combination with indentation depth as β. Using Eq. (6), different coated systems can now be compared in terms of the values of parameters β_0 and X. It is interesting and instructive to discuss the meaning of these parameters.

In order to appreciate the meaning of β_0, the relative indentation depth β can be set to this value. As a consequence, the ratio (β/β_0) becomes equal to unity, and the function f assumes a value of 0.5. Thus, β_0 is the value of the relative indentation depth at which the fractional hardness improvement is equal to exactly 50% of the maximum. Of course, alternatively this could be thought of as the RID at which the efficiency of using the coating is decreased by 50%. Variation of β_0 corresponds to the movement of the transition region along the E_0 axis, as illustrated in Fig. 5a for a fixed value $X = 3$. It could be argued that coated systems with larger values of β_0 would be preferred, since they sustain their hardness to larger indentation depths (and hence loads). In practice, the values of β_0 found in this and other studies all lie between 0.18 and 0.62.

The parameter X, on the other hand, describes how steeply the transition occurs between the extremes of hardness. For small values of X, the transition region extends over several decades of relative indentation depth. As the value of X is increased, the transition region becomes narrower, as illustrated in Fig. 5b for a fixed value $\beta_0 = 0.5$. In the limit of very large X the transition happens abruptly in the form of a step function.

4. Results and discussion

The body of experimental data presented here was obtained using micro- and macro-indentation of TiN,

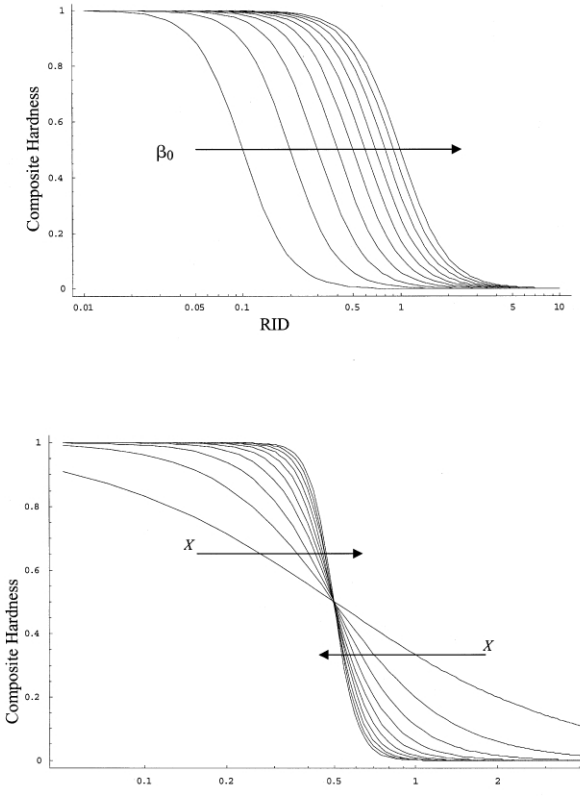

Fig. 5. Composite hardness plotted against RID. The value of X is fixed at 3; the curves represent the function for the values of β_0 between 0.1 and 1, increasing left to right. (b) Composite hardness plotted against RID. The value of β_0 is fixed at 0.5; the curves of increasing steepness represent the function for values of X varying between 1 and 10.

ZrN and TiCN coated samples, where heat-treated M2 tool steel was used as the substrate in all cases.

The first three columns in Table 1 show the coating used, the thickness of the coating and the hardness obtained through Vickers micro-indentation at a load of 100 g, $HV_{0.1}$. This is a standard load used for much of the current industrial characterisation and the results that follow demonstrate the problem encountered when comparing coated systems in this manner.

The remaining columns show the estimates obtained for the film hardness, H_f, the substrate hardness, H_s, and the dimensionless materials parameters k and X. From these values of k and X, the values of β_0 were calculated and included in the table. Of course, the choice of k or β_0 as the second parameter leads to entirely equivalent results, since the form of the model function is unchanged. However, significant benefits can be derived if β_0 is calculated, since it results in a clearer physical meaning of the fit, drastically reduced range of parameter variation, and much better predictive ability. Finally, the values of a parameter designated $\beta_{2/3}$ are also included in the table. The meaning of this parameter will be introduced below.

Fig. 2 shows the composite hardness (GPa) plotted against RID for a 2.8-μm NbN coating on M304 stainless steel. The data are taken from an earlier study [9], and combines nanoindentation, micro- and macrohardness testing results. It is clearly seen from the graph that the composite hardness levels out at a value very close to the substrate hardness at large penetration depths. However, no clear trend can be distinguished at very shallow penetration depths, since the variation takes place over a very small range of depth. In order to obviate this difficulty, it has become customary in the literature to employ logarithmic scale for the (relative) indentation depth [9–11,13,14]. Fig. 3 demonstrates that the result is a scale extended at low depths, and compressed for deep penetrations, i.e. precisely as required.

The measured data points are marked with diamonds and the model fit is shown as a dotted line. Fig. 3 illustrates the exceptional quality of the fit achieved between the model and the empirical nano-, micro- and macro-indentation data, with the correlation coefficient between the model and data being given by $R^2 = 0.994$. The fitting returns values of $H_f = 37.8 \pm 1.0$ GPa, $H_s = 2.7 \pm 0.4$ GPa, $k = 115 \pm 51$, and $X = 3.0 \pm 0.3$, from which the value of β_0 is calculated to be 0.20 ± 0.04.

Fig. 6 illustrates the fit to the micro- and macrohardness data only for 3.5 μm TiN coating on M2 tool steel. The correlation coefficient in this case is also $R^2 = 0.994$. The fitting returns values of $H_f = 32.3 \pm 1.1$ GPa, $H_s = 9.0 \pm 0.4$ GPa, $k = 7.8 \pm 2.1$ and $X = 1.9 \pm 0.2$, from which the value of β_0 is calculated to be 0.34 ± 0.02.

This finding is clearly in line with the estimate that

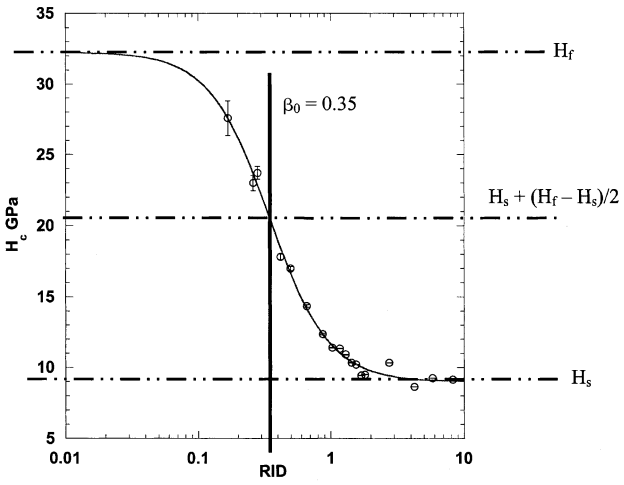

Fig. 6. Composite hardness plotted against RID for a 3.5-μm TiN coating on M2 tool steel. The superimposed horizontal lines represent H_f, at the top, H_s, at the bottom, and a line drawn half way between these values. β_0 is the point in RID where the composite hardness is half way between the hardness extremes and comes out at a value of approximately 0.35.

could be obtained from the graph (Fig. 6) using a simple graphical construction: a horizontal line drawn half way between the coating and substrate hardness levels. The corresponding abscissa gives the median value, β_0. Note that this result for β_0 ties in very well with our previous results on CrN coatings, which were obtained including reliable nanoindentation data (Fig. 17 [9]). We return to the discussion of this correlation later in this section.

Fig. 7 shows an SEM micrograph of a microhardness indentation in a ZrN-coated sample. Extensive coating cracking has taken place in the so-called 'picture-frame' pattern. This energy consumption mechanism is significantly different from the plastic deformation regime envisaged for the coating in the work-of-indentation analysis presented in the original paper [9]. This variation is likely to be responsible for the fact that the parameter X deviates from the value of 2 towards lower values in most of the fits described below.

In order to provide independent corroboration for the results obtained using different testing facilities, the same TiN sample (Fig. 6) was tested using two different micro-indentation devices, designated here Shimadzu and Buehler. The results of the two sets of measurements and the corresponding fits are shown in Figs. 6 and 8, respectively. The two plots are very similar, the second set of data (Fig. 8) yielding fit values of $H_f = 32.4$ GPa, $H_s = 9.2$ GPa, $k = 11.4$, $X = 1.7$, and $\beta_0 = 0.23$. The level of errors is once again similar. The details of all fitting results for all samples are presented in Table 1.

A similar plot showing composite hardness (GPa) against RID for a 3.6-μm TiN coating on M2 tool steel is shown in Fig. 9a. The figure includes the schematic

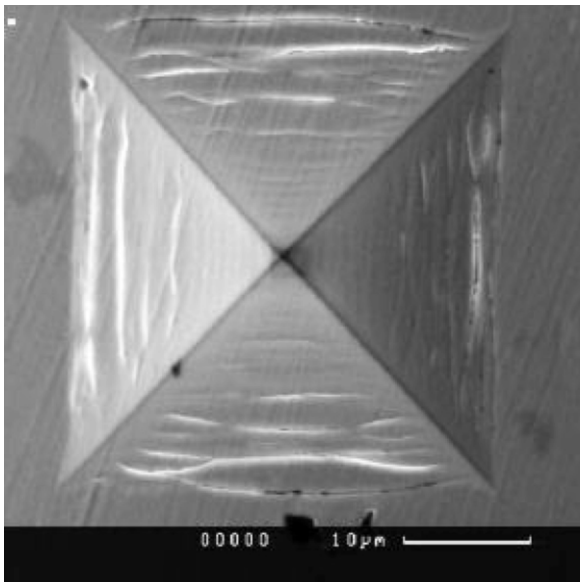

Fig. 7. An SEM micrograph of a 10-N (1 kg) Vickers indentation in a 4-μm ZrN coating on M2 tool steel substrate showing clearly the documented 'picture frame' fracture deformation. The indent corresponds to an indentation depth of 6.45 μm and RID of 1.6 μm.

estimation of β_0 values. The model fit to this set of data resolved values of $H_f = 29.9$ GPa, $H_s = 8.9$ GPa, $k = 10.9$, $X = 1.96$ and $\beta_0 = 0.3$. Once again, the measurements were also made using a different micro indenter, and the data obtained is shown in Fig. 9b. Model fitting to this set of data yielded results similar and values were returned for k, X and β_0, as 12.35, 1.45 and 0.18, respectively.

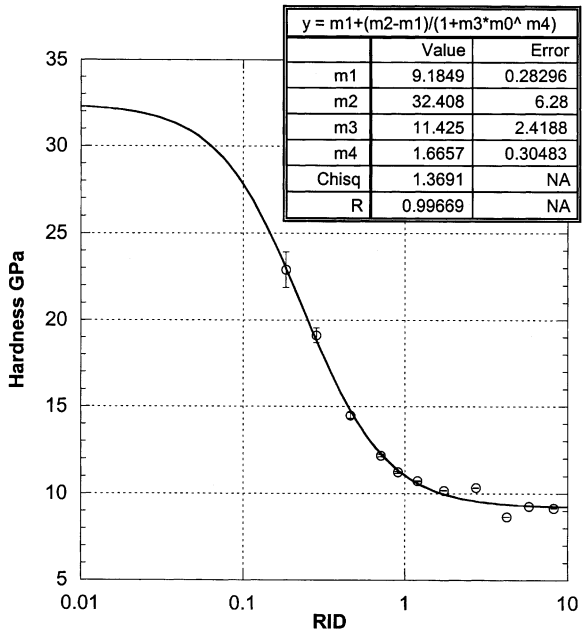

Fig. 8. Micro (Buehler) and macro indentation data collected from a 3.5-μm TiN coating on M2 tool steel. Hardness in GPa is plotted against RID.

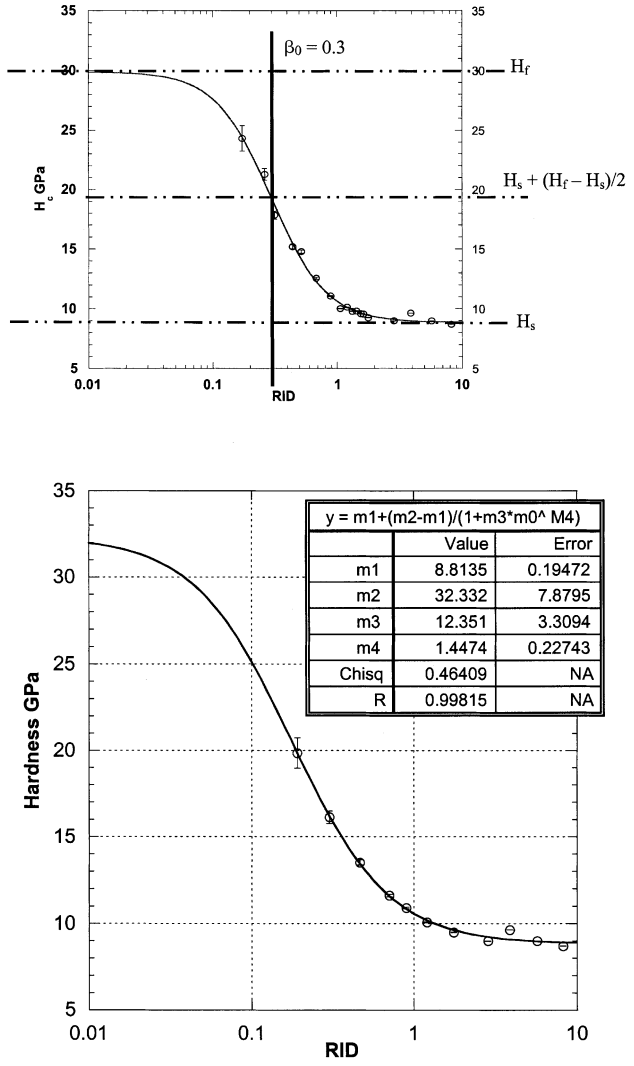

Fig. 9. (a) Micro (Shimadzu) and macro indentation data collected from a 3.6-μm TiN coating on M2 tool steel. Hardness in GPa is plotted against RID. The superimposed horizontal dashed lines represent the H_f and H_s levels, while the line shown between them is drawn at the 50% hardness increase level. Using this construction it is easy to establish from the plot that β_0 is equal to 0.3 (by drawing a vertical line through the intercept). This value of β_0 is representative of the values determined in this study based on the microhardness data alone. (b) Micro (Buehler) and macro indentation data collected from a 3.6-μm TiN coating on M2 tool steel. Hardness in GPa is plotted against RID.

Finally, for the TiN coated samples, Figs. 10 and 11 show the results for a 3.25-μm coating and a 3.75-μm coating, respectively. The model fitting is seen to conform well to the empirical data and the parameters are returned in good agreement with previous samples. The respective values of k lie between 4 and 12, and X between 1.45 and 1.96. β_0 values lie between 0.18 and 0.48.

For hardness values, it is expected that at a given load (for example, a current standard industrial characterisation at $HV_{0.1}$, or load 100 g), coatings with simi-

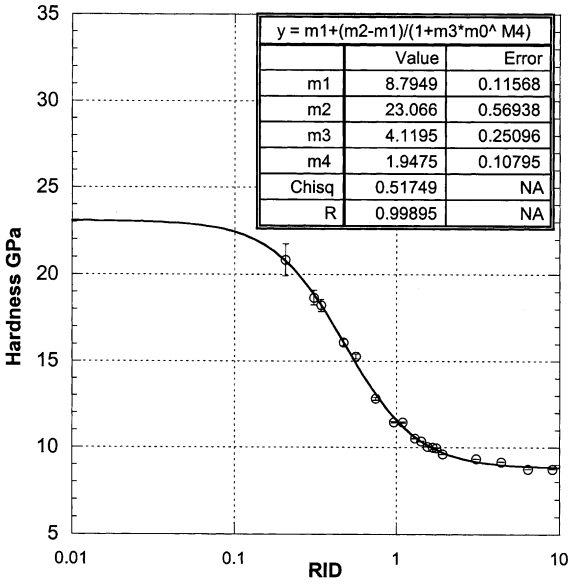

Fig. 10. Micro (Shimadzu) and macro indentation data collected from a 3.25-μm TiN coating on M2 tool steel. Hardness in GPa is plotted against RID.

larmicrostructure will give different hardness values when testing differing thicknesses, as shown. More explicitly, as the thickness of the similar coatings increases, and hence the coating plays more of a role in the energy expenditure during indentation, the hardness is expected to increase. In the case of these two coatings, quite the opposite is observed at low load (100 g) but when the ultimate film hardness is recovered it appears that the 3.25-μm coating now has a lower ultimate film hardness (23.1 GPa) than the 3.75-μm film (27.7 GPa). These observations would imply that the two coatings are not quite similar in their microstructure, due to the variation of deposition conditions, etc. If their values of k and X are considered it would appear that the value of k suggests that the 3.25-μm coating is less brittle than its opponent, and also possesses a reduced value of hardness. The value of X suggests that the transition between the two hardness extremes is more abrupt for this 3.25-μm film, again with implications towards the fracture properties of the two coatings. These observations thus allow some elucidation of the phenomenon observed during indentation testing, and move towards correlating the meaning of the parameters used in the present modelling approach with the system response. It also highlights the possible utility of such modelling approach for property characterisation and optimisation in industry.

The response from a 3.3-μm TiCN coating on M2 tool steel is shown in Fig. 12. The model fit again conforms well to the empirical data. This time the fitting parameters return values of $H_f = 56.1$ GPa, $H_s = 8.2$ GPa, $k = 15.8$, $X = 1.87$ and $\beta_0 = 0.24$. It can be seen from this plot that the TiCN sample has a far greater ultimate coating hardness than any of the TiN samples or ZrN samples later considered. Curve fitting resolves similar values with respect to X and β_0 but it is observed that k is significantly larger than the other samples considered in this study (TiN, ZrN). This ties in well with previously observed results that demonstrate that k is related to the fracture behaviour, and also the hardness of the coating [9–11,13,14].

Finally, also evaluated in this study was a set of ZrN coatings on M2 tool steel.

Fig. 13 shows the combined data from least square

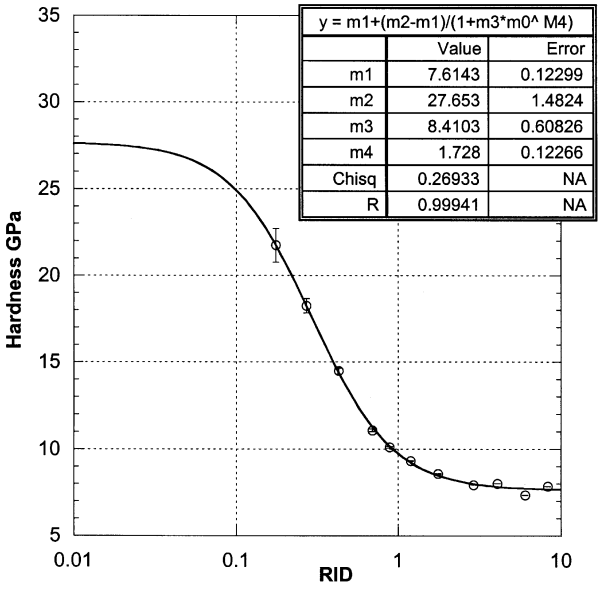

Fig. 11. Micro (Buehler) and macro indentation data collected from a 3.75-μm TiN coating on M2 tool steel. Hardness in GPa is plotted against RID.

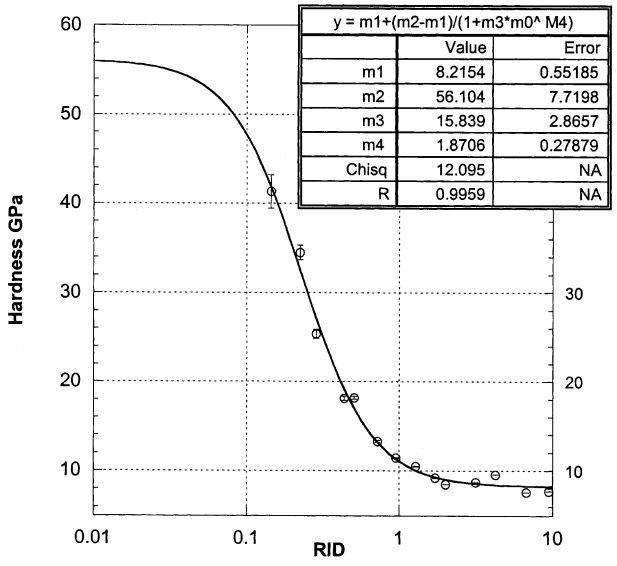

Fig. 12. Micro (Shimadzu) and macro indentation data collected from a 3.3-μm TiCN coating on M2 tool steel. Hardness in GPa is plotted against RID.

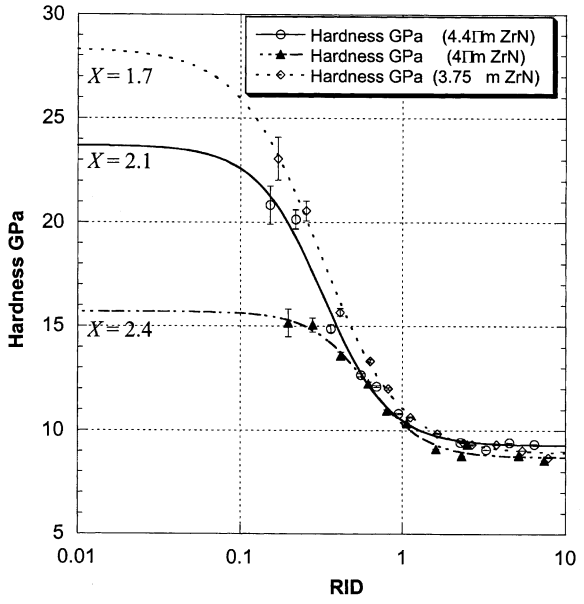

Fig. 13. Micro (Buehler) and macro indentation data collected from 4.4-, 4- and 3.75-μm ZrN coatings on M2 tool steel. Hardness in GPa is plotted against RID.

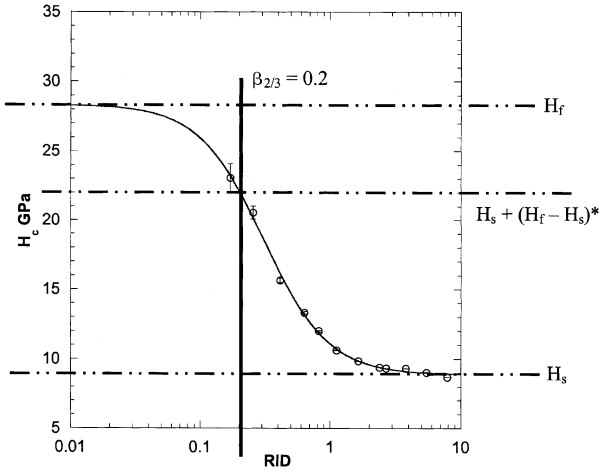

Fig. 14. Micro (Buehler) and macro indentation data collected from a 3.75-μm ZrN coating on M2 tool steel. Hardness in GPa is plotted RID. The superimposed horizontal dashed lines represent the H_f and H_s levels, while the line shown between them is drawn at the 66% hardness increase level. Using this construction it is easy to establish from the plot that $E_{2/3}$ is equal to 0.2 (by drawing a vertical line through the intercept). This value of $E_{2/3}$ is a representative example of the values determined in this study based on the microhardness data alone.

curve fits to the empirical data for ZrN coatings of 4.4 μm, 4 μm and 3.75 μm thickness, respectively. A similar trend is seen. In this case the k values are between 3.3 and 10.9, X values between 1.7 and 2.4 and β_0 values between 0.3 and 0.6. It is interesting to note that as the predicted film hardness increases, the value of X decreases from 2.4 (this is slightly over the originally proposed value of 2) to 1.7 (which is slightly lower than the originally proposed value). This highlights the need for allowing in the fit the variation of the parameter X, the exponent of β.

The last column in Table 1 represents a function $\beta_{2/3}$ that describes the value of RID at which the hardness improvement of approximately 66% is obtained. $\beta_{2/3}$ is represented in Fig. 14 in a similar fashion as before, where the plot shows composite hardness plotted against RID for a 3.75-μm ZrN coating on M2 tool steel. In the case for this ZrN coating, $\beta_{2/3}$ is equal to 0.2. For all the coatings considered, at this point, RID reaches an average of $0.23 \sim 0.2$, or approximately 20% of coating thickness.

It is interesting to note that an empirical rule has commonly been stated in the literature [16] that once the indentation depth reaches 1/10 of the coating thickness, the observation could be thought to describe the coating properties alone. Our present findings, however, raise important questions about the validity of this rule, and suggest possible restrictions and improvements. Fig. 15, constructed using the same data for the 3.75-μm ZrN coating, shows that at a depth of 1/10 the coating thickness, or RID = 0.1, we are observing only 88% of the hardness improvement compared with the predicted ultimate film hardness.

The results from micro and macro indentation testing of a range of cathodic filtered arc samples have been demonstrated here in correlation with the new fitting parameters β_0 and X, which modify the previously suggested work-of-indentation model fit to pro-

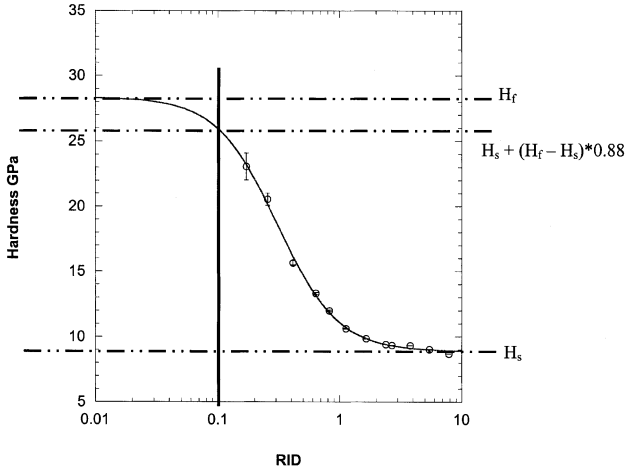

Fig. 15. Micro (Buehler) and macro indentation data collected from a 3.75-μm ZrN coating on M2 tool steel. Hardness in GPa is plotted against RID. The superimposed horizontal dashed lines represent the H_f and H_s levels, while the line shown between them is drawn at the 88% hardness increase level. Using this construction it is easy to establish from the plot that $\beta_{0.8}$ is equal to 0.1 (by drawing a vertical line through the intercept). This shows that at RID = 0.1, the operator is not dealing with the film properties alone.

vide us with something more meaningful. It is interesting here to revisit some original data used in the paper that introduced the work-of-indentation approach to modelling [9], to see exactly whether significant improvement to the fit quality is achieved, and whether marked difference exists between the new and old fitting parameters. For this purpose, some data collected from a 2.8-μm-thick NbN coating on M304 steel is used as shown in Fig. 16. The empirical data is marked with diamonds and a dashed line shows the originally proposed model fit ('the k-2 fit'). The corresponding returned parameters are shown in the top box. The new modelling approach is shown by a dotted line ('the k-X fit'); its returned parameters are given in the lower box. The new fitting approach, based upon the variation of k and X, can clearly be seen to conform better to the gradient of the empirical data. It gives what appears to be a more accurate representation for ultimate film hardness, in the absence of geometrical errors (tip shape, etc.) or those due to small-scale microstructure irregularities (size effect, etc.).

The final figure (Fig. 17) in the series presented is the composite hardness response of a 7.8-μm CrN coating on M304 steel, plotted against its RID. This figure is constructed using micro-indentation and reliable nano-indentation data, and is also drawn from the results presented previously by Tuck et al. [10]. It shows that when reliable nano-indentation data is used, the modelling is able to produce an adequate fit. It also

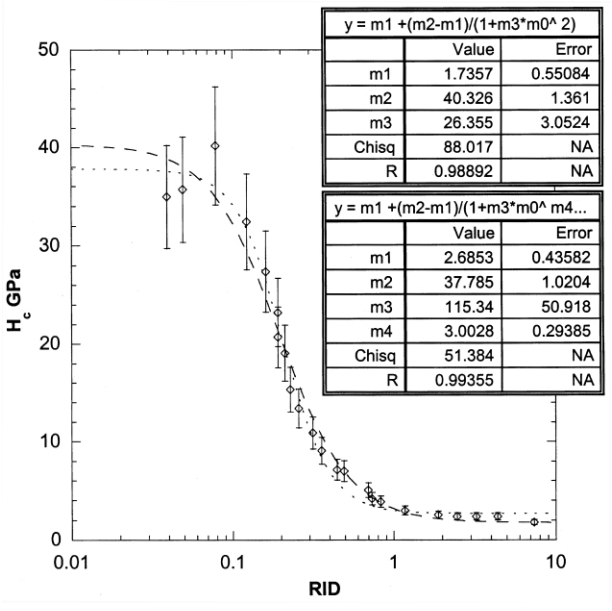

Fig. 16. Composite hardness plotted against RID for a 2.8-μm NbN coating on M304 steel. The two curves are comparisons between previous fitting routines using dimensionless materials parameter, k (shown by dashed line), and the newly developed techniques using parameters X and k (shown as a dotted line). The returned fitting parameters from each are shown top and bottom, respectively.

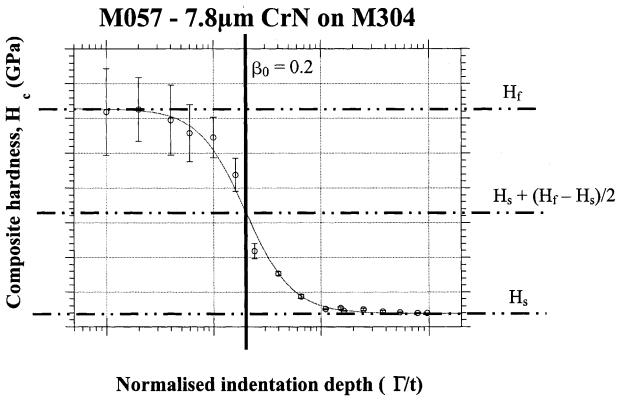

Fig. 17. Composite hardness plotted against RID for a 7.8-μm CrN coating on M304 steel. The experimental data from Korsunsky et al. [9] includes microhardness and nanoindentation measurements. The superimposed horizontal dashed lines represent the H_f and H_s levels, while the line shows between them is drawn at the 50% hardness increase level, i.e. corresponds to $H_s + (H_f + H_s)/2$. Using this construction it is easy to establish from the plot that E_0 is equal to 0.2 (by drawing a vertical line through the intercept). This value of β_0 is similar to the values presented in this study based on the microhardness data alone.

demonstrates that if a β_0 construction line is drawn at the point where RID is equivalent to a 50% increase in hardness, the value is found to be similar to those presented for the data studied in this paper (i.e. 0.2), which were based on micro-hardness analysis alone.

5. Conclusions

When indentation testing is performed at any one load or penetration depth, the full response of the system under study is not captured adequately for the purpose of characterisation. The approach based around work-of-indentation modelling of coated systems has been studied over the last few years [9–11,13,14,17]. In the present paper, two new fitting parameters have been proposed. Firstly, X, the exponent of E, the relative indentation depth. X is a parameter that describes how abruptly the response changes from ultimate film hardness to substrate hardness alone, on the RID scale. Secondly, a parameter β_0 which describes the depth, relative to the coating thickness, at which the response due to indentation shows half of the coating hardness improvement over the substrate. Thus, a greater versatility in fitting approach has been achieved, allowing more information to be extracted about the coated system from micro-hardness interpretation alone.

In the fitting approach, k and X are returned and β_0 is then calculated from these values. The results presented show that, firstly, data sets taken from the same system obtained on different micro-hardness machines provide reproducible fit. Also, values of β_0 that agree

with reliable nano-indentation results can be extracted when microhardness testing alone was used. It has been shown that the parameter X is strongly linked to the fracture deformation behaviour of the coating and that it can make a considerable difference if it is allowed to vary when using the model fit.

An introduction has also been made to the usefulness of the parameter β_0, and other related parameters. It has been shown in this work that predictions can be made for the load at which, for example, 66% of the hardness increase is obtained during indentation, thus giving a designer some guidance. For example, information of this kind could be used to decide how much more load the coated system could withstand before significant degradation of hardness occurs, or how much thicker it should be made in order to bear the required contact pressures without failure.

It is also shown that, contrary to earlier beliefs, when indented to a depth of 1/10th the coating thickness, the coated system response is not determined by the coating properties alone. For example, in the case of ZrN coatings considered in this study, only 88% of the maximum hardness improvement is attained, i.e. that at this contact depth the substrate continues to influence the response to a small degree.

Acknowledgements

JRT acknowledges the support of EPSRC in carrying out this work. AMK wishes to thank the Nuffield Foundation for the grant awarded under the New Lecturers in Science and Engineering scheme (NUF-NAL). Thanks are extended to the Design Unit, University of Newcastle upon Tyne, who provided the Buehler micro-indentation facility. JRT also wishes to thank Dr Ian Gilbert from the Department of Materials, University of Newcastle upon Tyne, for help and advice. This work was funded in part by a research grant from the Department of Energy, United States Government, under contract DE-FG02-98ER82702, to UES, Inc., Dayton, Ohio.

References

[1] R. Edwards, Cutting Tools, The Institute of Materials, 1993.
[2] V.I. Gorokhovsky, D.G. Bhat, Proceedings of the 1998 International Workshop on Surface Engineering and Coatings, Allied Publishers Ltd., Mumbai, India, 1999, pp. 381–399.
[3] B. Jonsson, S. Hogmark, Thin Solid Films 144 (1984) 257–269.
[4] P.M. Sargent, PhD thesis, University of Cambridge (1979).
[5] P.J. Burnett, D.S. Rickerby, Thin Solid Films 148 (1987) (41–50, 51–65).
[6] P.J. Burnett, T.F. Page, J. Mater. Sci. 19 (1984) 845–860.
[7] D.M. Marsh, Proc. R. Soc. A279 (1964) 420–435.
[8] S.J. Bull, D.S. Rickerby, Surf. Coat. Technol. 42 (1990) 149.
[9] A.M. Korsunsky, M.R. McGurk, S.J. Bull, T.F. Page, Surf. Coat. Technol 99 (1998) 171.
[10] J.R. Tuck, A.M. Korsunsky, S.J. Bull, Surf. Coat. Technol 127 (2000) 1–8.
[11] J.R. Tuck, A.M. Korsunsky, 13th European Conference on Fracture, San Sebastian, Spain, Sept 2000.
[12] D. Tabor, Rev. Phys. Technol. 1 (3) (1970) 145–179.
[13] J.R. Tuck, A.M. Korsunsky, S.J. Bull, R.I Davidson, Trans. Inst. Metal Finishing 78 (3) (2000) 105–109.
[14] J.R. Tuck, A.M. Korsunsky, S.J. Bull, R.I Davidson, Surf. Coat. Technol May (2000) (submitted).
[15] T.Y. Tsui, W.C. Oliver, G.M. Pharr, Mat. Res. Soc. (1996) 436.
[16] S.V. Hainsworth, T.F. Page, Thin Films: Stresses and Mechanical Properties VI, Materials Research Society Symposium Proceedings, 436 (1997), pp. 171–176.
[17] M.H. Staia, E.S. Puchi, G. Castro, F.O. Ramirez, D.B. Lewis, Thin Solid Films 355-356 (1999) 475–479.